Dramatic rate-enhancement of oxygen atom transfer by an iron(iv)-oxo species by equatorial ligand field perturbations

DOI:
10.1039/C8DT02142B

Document Version
Accepted author manuscript

Dalton Transactions

ARTICLE

Dramatic rate-enhancement of oxygen atom transfer by an iron(IV)-oxo species by equatorial ligand field perturbations

Received 00th January 20xx,
Accepted 00th January 20xx

DOI: 10.1039/x0xx00000x

www.rsc.org/

Gourab Mukherjee,[a] Calvin W. Z. Lee,[c] Sayanta Sekhar Nag,[a] Aligulu Alili,[c] Fabian G. Cantú Reinhard,[c] Devesh Kumar,[b] Chivukula V. Sastri*[a] and Sam P. de Visser*[c]

Nonheme iron dioxygenases are efficient enzymes with relevance for human health that regio- and stereospecifically transfer an oxygen atom to substrates. How they perform this task with such selectivity remains unknown, but may have to do with substrate binding, positioning and oxidant approach. To understand substrate approach on a catalytic reaction centre, we investigated the structure and reactivity of a biomimetic oxidant with ligand features that affect the interactions between oxidant and substrate. Thus, we report here the synthesis and characterization of an iron(IV)-oxo complex with pentadentate nonheme ligand, where structurally induced perturbations in the equatorial ligand field affect the spectroscopy and reactivity of the complex. We tested the activity of the complex with respect to oxygen atom transfer to and hydrogen atom abstraction from substrates. This oxidant shows improved reaction rates toward heteroatom oxidation with respect to the nonsubstituted ligand complex by ~10^4 fold. The origin of the enhanced reactivity is explained with a series of density functional theory studies that show an enhanced electron affinity of the oxidant through equatorial ligand perturbations.

Introduction

Iron-containing metalloenzymes are well-known oxidants that carry out metabolically vital oxidative transformations in the human body.[1] High valent iron(IV)-oxo complexes have often been identified as the key reacting species in such oxidative transformations,[2] and indeed have been characterized for several nonheme iron dioxygenases.[3] Most nonheme iron dioxygenases display a typical facial iron coordination via two histidine and one carboxylate based residue; usually from Asp or Glu. Many details on the catalytic reaction mechanisms of heme and nonheme metalloenzymes remain unknown. Moreover, many nonheme iron dioxygenases react with substrates in a stereoselective or regiospecific manner. For instance, prolyl-4-hydroxylase activates a proline residue in a peptide chain to give solely the R-4-hydroxyproline product as part of its natural biosynthesis pathway.[4] Recent QM/MM studies showed that even though 5-hydroxyproline would be a thermodynamically more stable product, the enzyme manages to avoid this product through substrate binding and orientation.[5] In particular, substrate is held in a tight binding pocket and can only approach the active site through a narrow funnel lined up by a Trp and Tyr residue. Moreover, key hydrogen bonding interactions hold the substrate in a tight conformation and site-selective mutations of one of the residues in the substrate binding pocket leads to either loss of specificity or complete loss of activity. Other enzymes with tight substrate binding pockets that catalyse a regioselective reaction include the camphor hydroxylating heme enzyme cytochrome $P450_{cam}$,[6] and the nonheme iron dioxygenase AlkB, which is involved in DNA repair mechanisms through the demethylation of methylated DNA bases.[7] Clearly, the substrate binding position and orientation in enzymes is important and can determine and affect the product distributions.

To understand the mechanistic aspects of metalloenzymes biomimetic models have been developed that contain the coordination features of the metal but lack the protein environment.[8] Artificial/synthetic mimics of these biological systems provide necessary information about their catalytic cycle and their mode of operation. There are several reports in the literature regarding the tuning of the primary coordination sphere of these high valent intermediates and the various factors that affect their reactivity, such as ligand topology, axial ligation, spin-state of the metal atom, etc.[9] As changes in the primary coordination sphere can be quite dramatic, research has also focused on the influence of secondary coordination sphere modifications, where changes are more

[a] Department of Chemistry, Indian Institute of Technology Guwahati, Assam 781039, India. Fax: +91-361-258-2349; E-mail: sastricv@iitg.ernet.in.
[b] Department of Applied Physics, School for Physical Sciences, Babasaheb Bhimrao Ambedkar University, Lucknow 226025, India. E-mail: dkclcre@yahoo.com.
[c] The Manchester Institute of Biotechnology and the School of Chemical Engineering and Analytical Science, The University of Manchester, 131 Princess Street, Manchester M1 7DN, United Kingdom. E-mail: sam.devisser@manchester.ac.uk.

† Footnotes relating to the title and/or authors should appear here.
Electronic Supplementary Information (ESI) available: Experimental and computational raw data, including Cartesian coordinates of optimized structures, absolute and relative energies and group spin densities and charges. See DOI: 10.1039/x0xx00000x

subtle.[10] Non-covalent interactions in the vicinity of the active site, such as charge induction or stereochemical perturbations influence reaction mechanisms and can change bifurcation pathways.[11]

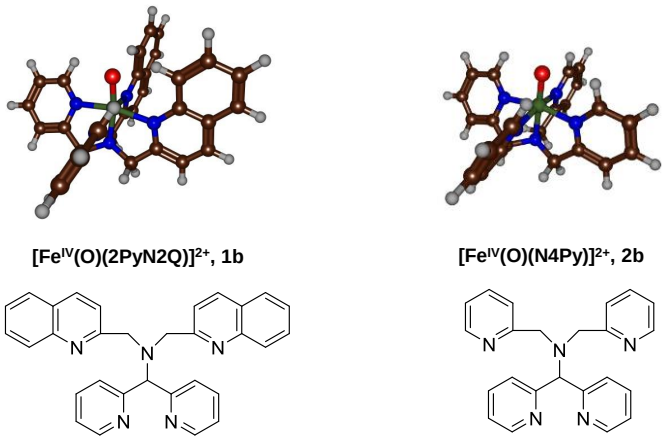

Fig. 1. Oxidants investigated in this study.

A biomimetic iron(IV)-oxo species that has received quite a lot of attention over the years is the [Fe^{IV}(O)(N4Py)]$^{2+}$ complex with N4Py = N,N-bis(2-pyridylmethyl)-N-bis(2-pyridyl) methylamine): structure **2b** in Fig. 1. The complex was originally synthesized by Feringa and Que and their co-workers[12] and was one of the first biomimetic iron(IV)-oxo species that was characterized by electron paramagnetic resonance, resonance Raman, Mössbauer, UV-vis and nuclear magnetic resonance (NMR) spectroscopic methods as well as by X-ray crystallography.[13] In addition, many reactivity studies with substrates have been reported, which showed it efficiently reacts through oxygen atom transfer.[14] Very recently Que and co-workers showed that substitution of the three pyridine rings of the tetradentate TPA, tris-(2-pyridylmethyl)amine, ligand by quinoline moieties enabled the synthesis of a high-spin (S = 2) iron(IV)-oxo species.[15] However, replacement of the pyridine rings by N-methylbenzimidazole moieties, instead generated an S = 1 iron(IV)-oxo ground state.[16] Nevertheless, in both of these systems enhanced reactivity towards substrates was observed. Interestingly, such ligand modifications are much less explored in pentadentate iron(IV)-oxo intermediates. Nordlander and co-workers have shown that a systematic replacement of the pyridine groups with N-methylbenzimidazole in the N4Py ligand framework leads to enhanced reaction rates.[17]

In particular, the introduction of *ortho*-substituents to a pyridine ring is a well-established design strategy to significantly affect the iron(IV)-oxo core by weakening the Fe–N_{eq} bonds. To gain insight into the influence of the equatorial ligand perturbations in biomimetic complexes, we engineered the N4Py ligand system to 2PyN2Q (1,1-di(pyridin-2-yl)-N,N-bis(quinolin-2-ylmethyl)methanamine). The introduction of bulky quinoline moieties is expected to influence the electronic orbitals and spectroscopic features of the iron(IV)-oxo oxidant and hence its reactivity with substrates. Specifically, we compare the spectroscopy and reactivity of the two nonheme iron(IV)-oxo complexes **1b** and **2b** (Fig 1), namely [Fe^{IV}(O)(2PyN2Q)]$^{2+}$ and [Fe^{IV}(O)(N4Py)]$^{2+}$. In these complexes the equatorial ligand perturbations on the oxo group are different, whereby in **1b** the oxo group undergoes two weak C-H--O hydrogen bonding interactions that is absent in complex **2b**. We predicted that the changes in ligand coordination may give different spectroscopic and reactivity patterns. Indeed, the results described in this work show a dramatic rate-enhancement with the new ligand system, which is explained through a combination of experimental and computational studies.

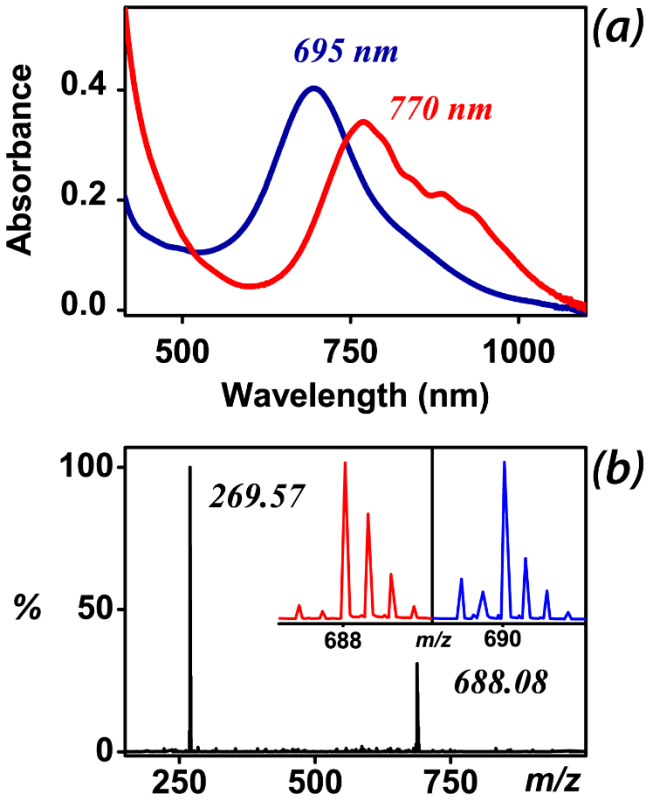

Fig 2. a) UV-vis spectra of **1b** (red) and **2b** (blue) in CH_3CN at 298 K; b) Electrospray Ionization mass spectra of **1b** in CH_3CN at 298 K. Inset shows expanded isotopic distribution pattern of [Fe^{IV}(O^{16})(2PyN2Q)(OTf)]$^+$ (red) and [Fe^{IV}(O^{18})(2PyN2Q)(OTf)]$^+$ (blue).

Results and discussion

In this work we report a combined experimental and computational study on the reactivity of a modified N4Py ligand system (2PyN2Q) that when bound to an iron(IV)-oxo influences substrate approach and therefore leads to significant enhancement of oxidative properties. Various experiments are performed to understand the mechanism of the reaction and are supported by computational studies.

Experiment.

Our initial work started from a pentadentate nonheme iron complex [Fe^{II}(2PyN2Q)(OTf)$_2$], **1a**, supported by the 2PyN2Q ligand bearing quinoline moieties.[18] Dropwise addition of an acetonitrile solution containing Fe^{II}(OTf)$_2$•2CH_3CN to the ligand

resulted in the formation of a dark yellow compound (**1a**) in 95% yield that could be characterized with UV-vis spectroscopy, electrospray ionization-mass spectrometry (ESI-MS) and NMR spectroscopy, see Figs. S2 and S3 (Electronic Supporting Information). Treatment of **1a** with 1.5 equivalents of $PhI(OAc)_2$ in CH_3CN under ambient conditions generated the corresponding iron(IV)-oxo complex $[Fe^{IV}(O)(2PyN2Q)]^{2+}$, **1b** ($\lambda_{max}$ = 770 nm, ε = 340 L M^{-1} cm^{-1}, $t_{1/2}$ = 50 min at RT), Fig. 2a. These values are similar to those reported recently by Que et al.[19] The intermediate **1b** was also prepared by the addition of PhIO (in CF_3CH_2OH) and 1-^{t}butylsulfonyl-2-iodosylbenzene with a half-life of 3 and 50 min respectively. The UV-vis absorption spectrum of **2b** when generated under the same experimental conditions gave an absorption band at λ_{max} = 695 nm with a half-life of over 60 hours typical of $[Fe^{IV}(O)(N4Py)]^{2+}$. Thus, substitution of the pyridine rings in N4Py with quinoline groups to form 2PyN2Q resulted in a bathochromic shift of the d-d transition band by 75 nm and a significant loss of the thermal stability of the complex. These lifetimes indicate that the ligand architecture at the equatorial site influences its stability and reactivity.

The ESI-MS gives a major peak at *m/z* 269.57 corresponding to $[Fe^{IV}(O)(2PyN2Q)]^{2+}$ and a minor peak at *m/z* 688.08 representing the $[Fe^{IV}(O)(2PyN2Q)(OTf)]^{+}$ ion (Fig. 2b). The isotopic patterns for the two species confirm the assignments of the two ions. The formation of $[Fe^{IV}(O)(2PyN2Q)]^{2+}$ was further established by an isotopic labelling experiment using $H_2{}^{18}O$, which leads to oxygen atom exchange with the oxo group. The experiment with $H_2{}^{18}O$ moves the peak in the ESI mass spectrum for $[Fe^{IV}(O)(2PyN2Q)(OTf)]^{+}$ from *m/z* 688.08 to *m/z* 690.08, while the peak representing the $[Fe^{IV}(O)(2PyN2Q)]^{2+}$ ion shifts by one unit. Hence the isotopic labelling experiment shows that one oxygen atom is incorporated into the metal complex in the form of an iron(IV)-oxo. We further employed ^{1}H-NMR spectroscopy to see the differences between the two iron(IV)-oxo complexes (see Fig. S3, Electronic Supporting Information). The ^{1}H-NMR spectra for complex **2b** as reported by Klinker et al reveals the presence of mirror symmetry.[13b] However, for complex **1b,** as expected, a more complicated spectrum with a larger number of signals is obtained compared to **2b,** due to the presence of quinoline groups instead of pyridine rings. The observed range of paramagnetic shift in the ^{1}H-NMR spectrum of **1b** decreased with respect to its Fe(II) precursor and gave a typically *S* = 1 shift.[10a,13b,20] To gain more insight into the electronic structure of **1b**, we performed a variable temperature NMR experiment over a temperature range from 233 – 298 K. With a lowering of the temperature, no upfield shift of peaks was observed in the Curie plot, thereby confirming an *S* = 1 ferryl species as the ground state, see Figs. S4 and S5 (Electronic Supporting Information). This observation was further supported by a recent report of Rasheed et al using Mössbauer spectroscopy.[19] The Fourier transform infrared spectral data of **1b** showed a Fe=O stretch vibration at 834 cm^{-1} which was at a lower frequency in comparison with **2b**.[19] Nevertheless, the lifetime of **1b** is sufficiently long to enable us do a detailed kinetics and spectroscopy study at room temperature alongside those for the analogous complex **2b**, i.e. $[Fe^{IV}(O)(N4Py)]^{2+}$.

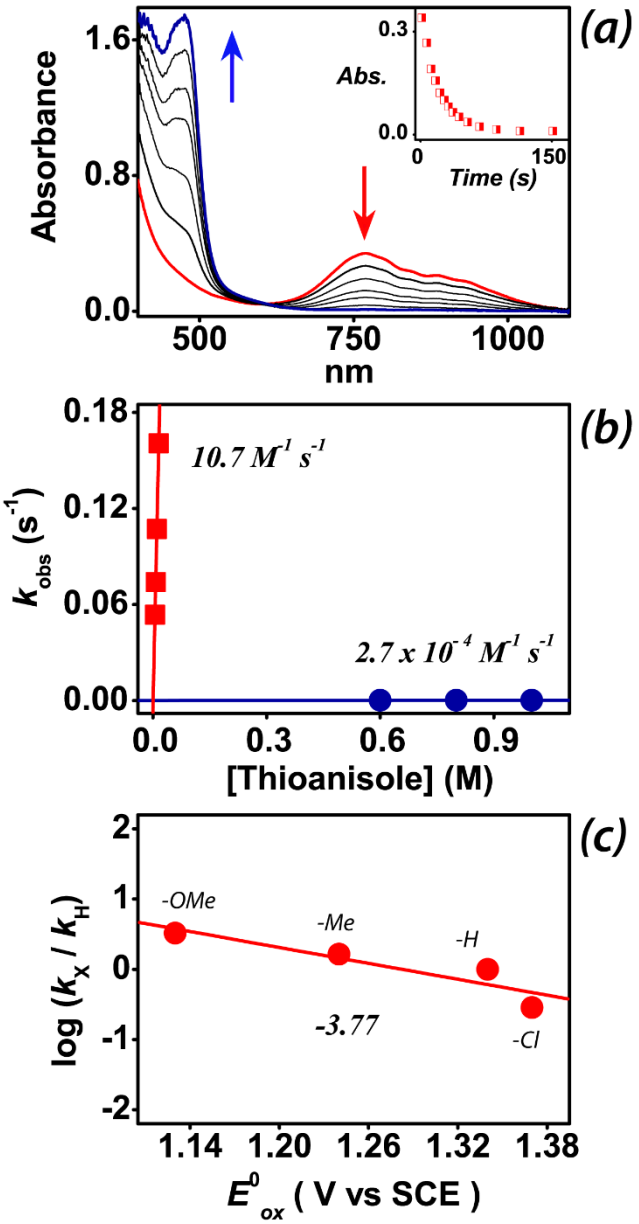

Fig 3. a) UV-vis spectral changes of **1b** upon addition of 7 equiv. thioanisole in CH_3CN at 233 K. Inset shows the decay profile of the 770 nm band; b) Second order rate constant determined for the reaction of **1b** (1mM) (■) and **2b** (1 mM) (●) with thioanisole at 233 K; c) Plot of log (k_X/k_H) against one-electron oxidation potentials (E^0_{ox}) of *p*-X-thioanisols in their reaction with **1b** (●) at 233 K in CH_3CN, where k_X and k_H are the pseudo first-order rate constants of *p*-X-thioanisole and thioanisole, respectively.

Table 1. Pseudo first-order rate constants (k_{obs}) determined for the reaction of **1b** (1 mM solution in CH_3CN) with 5 equivalents of *para*-X-substituted thioanisole at –40 °C in CH_3CN.[a]

X [b]	σ_P [c]	σ_P^+ [c]	E^0_{ox} [d]	k_{obs} [e]	k_X/k_H [f]	$\log(k_X/k_H)$
$-OCH_3$	-0.27	-0.78	1.13	0.177(4)	3.29	0.52
$-CH_3$	-0.17	-0.31	1.24	0.088(2)	1.64	0.22
-H	0.00	0.00	1.34	0.054(2)	1.00	0.00
-Cl	0.23	0.11	1.37	0.015(3)	0.28	-0.55.

[a] All the reactions were followed by monitoring the UV-vis spectral changes of the reaction solution. [b] *para*-substituents in *para*-X-thioanisole. [c] data taken from Ref 21a. [d] data taken from Ref 21b. [e] In s^{-1}. [f] Relative rate constant obtained by dividing the k_{obs} of *p*-X-thioanisole by k_{obs} of *p*-H-thioanisole.

Table 2. C–H Bond dissociation energies and second-order rate constant values for the reaction of **1b** (1 mM) and **2b** (1 mM) with various substrates in CH_3CN at 25 °C.

Substrate [a]	BDE_{C-H} (kcal mol^{-1}) [b]	Complex	k_2 [c]	k_2' [c,d]	log k_2'
Ph_3CH (1)	81	**1b**	0.376(4)	0.376	-0.42
		2b	0.043(2)	0.043	-1.37
$PhCH(CH_3)_2$ (1)	84.5	**1b**	0.125(3)	0.125	-0.90
		2b	0.003(3)	0.003	-2.55
$PhCH_2CH_3$ (2)	87	**1b**	0.082(2)	0.041	-1.38
		2b	0.011(1)	0.005	-2.26
$PhCH_3$ (3)	90	**1b**	0.015(4)	0.005	-2.29
		2b	0.0006(2)	0.0002	-3.68

[a] The number in the parenthesis indicates the number of equivalent H-atoms on the substrate that would react with the iron(IV)-oxo species. [b] from Ref 13. [c] In M^{-1} s^{-1}. [d] The k_2' values are obtained by dividing k_2 values by the number of equivalent hydrogen atoms in the substrate that would react with the iron(IV)-oxo species.

In order to find out whether the change in spectroscopic properties of the oxidant (**1b** versus **2b**) has an effect on the oxidation properties, we did a thorough kinetics study using a range of different substrates. Thus, we employed thioanisole and benzyl alcohol as model substrates for heteroatom oxidation and alcohol oxidation reactions, respectively.

Addition of thioanisole to **1b** at 233 K led to the decay of the iron(IV)-oxo characteristic band at 770 nm in the UV-vis spectrum concomitant with the appearance of its iron(II) precursor (λ_{max} = 475 nm) with an isosbestic point at 605 nm, thereby generating methyl phenyl sulfoxide as the major product (Fig. 3a). We measured the change in absorbance from the UV-vis spectra at 770 nm and plotted it as a function of time, which enabled us to determine the pseudo first-order rate constant (k_{obs}) for the reaction. Subsequently, these observed rate constants were converted into second-order rate constants by plotting k_{obs} as a function of substrate concentration. The second-order rate constant (k_2) for the reaction of thioanisole with **1b** was evaluated to be 10.7(4) M^{-1} s^{-1} at 233 K (Fig. 3b). Previous work on the reaction of thioanisole with **2b** under the same reaction conditions,[16] provided a second-order rate constant of 2.7×10^{-4} M^{-1} s^{-1}. Consequently, under the same experimental conditions, *the reactivity of **1b** with thioanisole is faster than that of **2b** by a factor of almost 4×10^4 fold*. This rate increment is much higher than those observed for an analogous ligand system with N-methylbenzimidazole substituents by at least 30 times.[17] The enhanced reaction rate probably originates from the introduction of the *ortho*-substituent on the pyridine ring and consequent weakening of the $Fe–N_{eq}$ bonds relative to that in **2b**. To gain insight into the mechanistic details of the reaction, we studied the reaction of **1b** with various *para*-X-substituted thioanisole substrates (X = OCH_3, CH_3, H, Cl) and measured their reaction rates (Table 1 and Fig. S6, Electronic Supporting Information).[21] A plot of the logarithm of the rate constant ratio (k_X/k_H) as a function of the one-electron oxidation potentials (E^0_{ox}) of various *para*-X-substituted thioanisole substrates gives a linear correlation with a slope of ρ = –3.77 (Fig. 3c). The negative ρ value and slope implicates that the reaction proceeds via atom transfer through an electrophilic reaction mechanism.[21b]

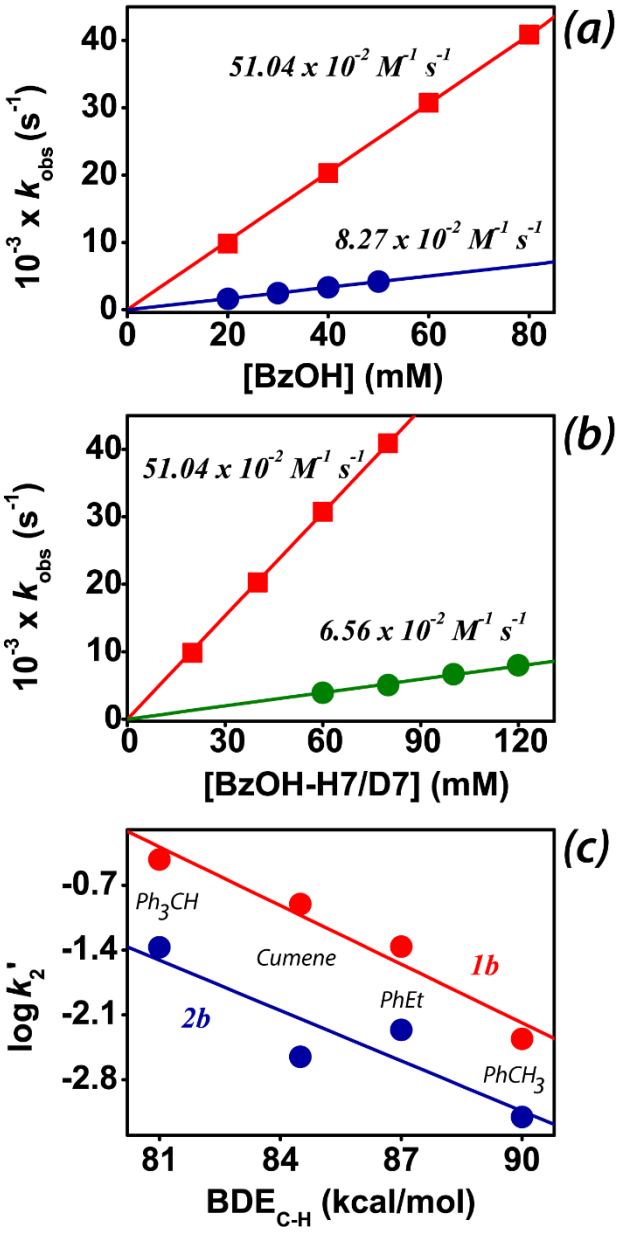

Fig 4. Second-order rate constant determined for the reaction of a) 1 mM **1b** (■) and 1mM **2b** (●) with benzyl alcohol in CH_3CN at 298 K; b) 1mM **1b** with benzyl alcohol (■) and benzyl alcohol-d_7 (●) in CH_3CN at 298 K; c) Correlation between C–H bond dissociation energies of different hydrocarbons and log k_2' for their reactions with **1b** (●) and **2b** (●) at 298 K; k_2' is the second–order rate constant divided by the number of equivalent C–H bonds on the substrate that would react with the iron(IV)-oxo.

To compare the reactivity difference of **1b** over **2b** in C–H activation reactions, we subsequently monitored the hydrogen atom abstraction ability of both complexes toward benzyl alcohols. Upon addition of different concentrations of benzyl alcohol to **1b** in acetonitrile, the 770 nm band decayed in a pseudo first-order manner as a function of time. Product analysis reveal the formation of benzaldehyde in almost stoichiometric yields (>80% with respect to intermediate formed). The second-order rate constant (k_2) for the reaction of **1b** with benzyl alcohol is found to be 51.04(1) $\times$ 10^{-2} M^{-1} s^{-1} at 298 K (Fig. 4a), whereas previous work for **2b** found a value of 8.27 $\times$ 10^{-2} M^{-1} s^{-1} under the same reaction conditions.[22] As such, $[Fe^{IV}(O)(2PyN2Q)]^{2+}$ reacts with benzyl alcohol with rates that are more than six times faster than $[Fe^{IV}(O)(N4Py)]^{2+}$. Therefore, the equatorial ligand environment has significant effect on the reaction rates of alcohol oxidation reactions. Its rate-enhancement, however, is not as strong as in oxygen atom transfer (compare Fig. 3b and Fig. 4a), but clearly both reaction processes are favoured with **1b** as an oxidant.

To ascertain that hydrogen atom abstraction is indeed the rate-determining step in the reaction mechanism, we repeated the experiment with benzyl alcohol-d_7 or $C_6D_5CD_2OH$ as the substrate. A comparison of the rate constants depicted in Fig. 4b (and Table S1, Electronic Supporting Information) clearly shows that substitution of the active hydrogen atom by deuterium reduces the reaction rate by a factor of about 8. Hence, we determine a kinetic isotope effect (KIE) value of 8 for the reaction of **1b** with benzyl alcohol at 298 K. This KIE value is indicative of a rate-determining hydrogen atom abstraction step in the reaction mechanism. Our mechanism, therefore, is in excellent agreement with that derived for **2b** with benzyl alcohol although an even larger KIE value is obtained upon replacement of hydrogen by deuterium.[22,23]

We then studied the hydrogen atom abstraction ability of **1b** and **2b** with a selection of substrates with known C–H bond strengths. Previously, it was shown that reactions proceeding with a rate-determining hydrogen atom abstraction have the natural logarithm of the rate constant linearly related to the C–H bond dissociation energy (BDE_{C-H}).[24] We investigated the hydrogen atom abstraction reactions of **1b** with substrates including triphenylmethane, cumene, ethylbenzene and toluene (Fig. 4c and Table 2). These substrates span a range of C–H bond dissociation energies (BDE_{C-H}) typical for hydrogen atom abstraction reaction rates.[13a,25] As can be seen from Fig. 4c, a linear correlation between the natural logarithm of the rate constant versus BDE_{C-H} is found for the reactions of **1b**/**2b** with substrates. The linearity of the Bell-Evans-Polanyi plot (log k_2' versus BDE_{C-H}) provides evidence of a rate-determining hydrogen atom abstraction. Product analysis of the dead reaction mixture after the decay of the characteristic band in UV-vis spectrum indicated the production of the corresponding alcohols (and aldehydes) in variable yields (e.g. Ph_3C–OH, 88%; $PhC(OH)(CH_3)_2$, 60%; $PhCH(OH)CH_3$, 32% and PhCHO, 55%). It is not surprising to see that the rate enhancement for sulfoxidation is different from hydrogen atom abstraction as sulfoxidation generally is a concerted two-electron reaction mechanism, whereas substrate hydroxylation is stepwise reaction via a radical intermediate.[26] Clearly, the change of the ligand and the introduction of equatorial ligand perturbations do not affect the reaction mechanism of **1b**/**2b** with substrates. However, the change in ligand does affect the absolute reactivities.

Further evidence of the mechanism was obtained through studies of *para*-X-substituted benzyl alcohols in a reaction with $[Fe^{IV}(O)(2PyN2Q)]^{2+}$, **1b**. In particular, we monitored the influence of electron-withdrawing or electron-donating *para*-

X-substituents on the reaction rate of **1b** with benzyl alcohols at 298 K. When we plot the log (k_X/k_H) values as a function of the Hammett parameters, σ_p, a linear trend is found with a slope of ρ = –0.27, Fig. S7 and Table S2 (Electronic Supporting Information). This small Hammett ρ value implicates little electronic effects as a result of the addition of *para*-substituents to the benzyl alcohol. Mechanistically, therefore, **1b** shows a reactivity pattern close to that previously reported on **2b**, where a ρ value of –0.10 was found under similar reaction conditions.[22]

Finally, a reactivity study of **1b** with cyclobutanol was performed, which is often used as a mechanistic probe.[22,23] In particular, formation of cyclobutanone as a product indicates a single step two-electron process, whereas two sequential one-electron steps involve ring opening of the substrate and the subsequent formation of 4-hydroxybutyraldehyde. We find that **1b** reacts with cyclobutanol to give cyclobutanone as the major product, thereby, confirming that alcohol oxidation by complex **1b** proceeds by a direct two-electron transfer pathway.

Theory.

In order to understand the rate-enhancement of **1b** over **2b** in oxygen atom transfer reactions, we initiated a density functional theory (DFT) study using methods and procedures calibrated against experimental rate constants for $[Fe^{IV}(O)(N4Py)]^{2+}$ reactivities previously.[22,27] Our previous studies reproduced experimental free energies of activation to within 3 kcal mol^{-1} using the methods and procedures used here.[28] Particularly, test calculations using about 50 different computational methods and basis sets showed that B3LYP/BS2//B3LYP/BS1 with solvent corrections was one of the best performing procedures.[27b] Further tests using this procedure found good structures and potential energy landscapes that were generally within 0.5 kcal mol^{-1} of those obtained with B3LYP/BS2.[29] This was indeed confirmed here for the toluene reaction mechanism (see Electronic Supporting Information). Furthermore, in case of bifurcation pathways leading to multiple products, the methods predicted the correct product distributions for the reactivities of nonheme iron(IV)-oxo complexes and consequently correct transition state ordering.[30]

We started with a detailed analysis of the electronic and structural configuration of **1b** or $[Fe^{IV}(O)(2PyN2Q)]^{2+}$ in the triplet and quintet spin states, see Fig. 5. At the ΔE+ZPE level of theory with solvent corrections included, the triplet spin state is the ground state by 2.8 kcal mol^{-1}. This energy difference is considerably smaller to that found for ^{3,5}**2b** or $^{3,5}[Fe^{IV}(O)(N4Py)]^{2+}$, where a value of 7.5 kcal mol^{-1} was found using the same methods.[22,31] Interestingly, the structural differences between ^{3}**1b** and ^{3}**2b** are relatively minor with similar Fe–O distances (1.658 vs 1.660 Å). The only changes appear to be a drop in the Fe–O stretch vibration (859 vs 846 cm^{-1}) and a more tilted O–Fe–N_{axial} angle (from 179.5° to 171.3°) for ^{3}**2b** versus ^{3}**1b**, respectively.

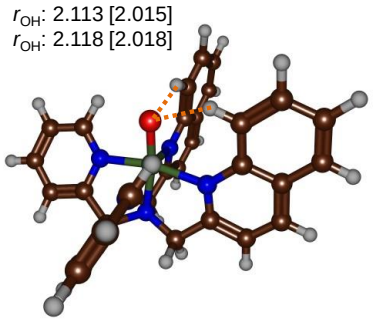

Fig. 5. UB3LYP/BS1 optimized geometries of ^{3,5}**1b** as obtained in Gaussian. Bond lengths are in angstroms and angles in degrees.

The geometric differences between ^{3}**1b** and ^{3}**2b** can affect the high-lying occupied and low-lying virtual orbitals and hence influence physical variables such as electron affinity (EA), ionization energy (IE) and proton affinity. To highlight the differences in high-lying occupied molecular orbitals we display orbital diagrams of ^{3}**1b** and ^{3}**2b** in Fig. 6. This Figure displays the metal-type molecular orbitals of ^{3}**1b** and ^{3}**2b** and particularly focus on orbitals that include an iron 3d contribution that interacts with neighbouring atoms. The lowest in energy are the bonding pair of orbitals (π_{xz}/π_{yz}) for the interaction of the metal $3d_{xz}/3d_{yz}$ with the $2p_x/2p_y$ on oxygen. A little bit higher in energy is the π^*_{xy} molecular orbital, which is perpendicular to the Fe–O axis inside the plane of the four pyridine nitrogen atoms. In heme-type iron complexes this π^*_{xy} orbital is nonbonding and generally labelled as δ,[32] but here interactions are seen with the aromatic groups of the 2PyN2Q ligand. These antibonding interactions will raise the π^*_{xy} in energy and may result in a stabilization of the quintet spin state as seen from the relative energies. A bit higher in energy than the π^*_{xy} orbital are the almost degenerate π^*_{xz} and π^*_{yz} molecular orbitals for the antibonding interaction of the metal $3d_{xz}/3d_{yz}$ atomic orbital with the $2p_x/2p_y$ atomic orbital of the oxo group. Also these two orbitals interact with orbitals on the aromatic 2PyN2Q ligand system and particularly with the hydrogen atoms that hydrogen bond with the oxo group. Higher in energy and virtual in the triplet spin state are two σ^* orbitals, namely the σ^*_{z2} orbital for the antibonding Fe–O interaction and the σ^*_{x2-y2} orbital for the interaction of iron with four nitrogen atoms. The latter is the only molecular orbital where few or little extra interactions between the metal and ligand are observed.

Dalton Transactions

ARTICLE

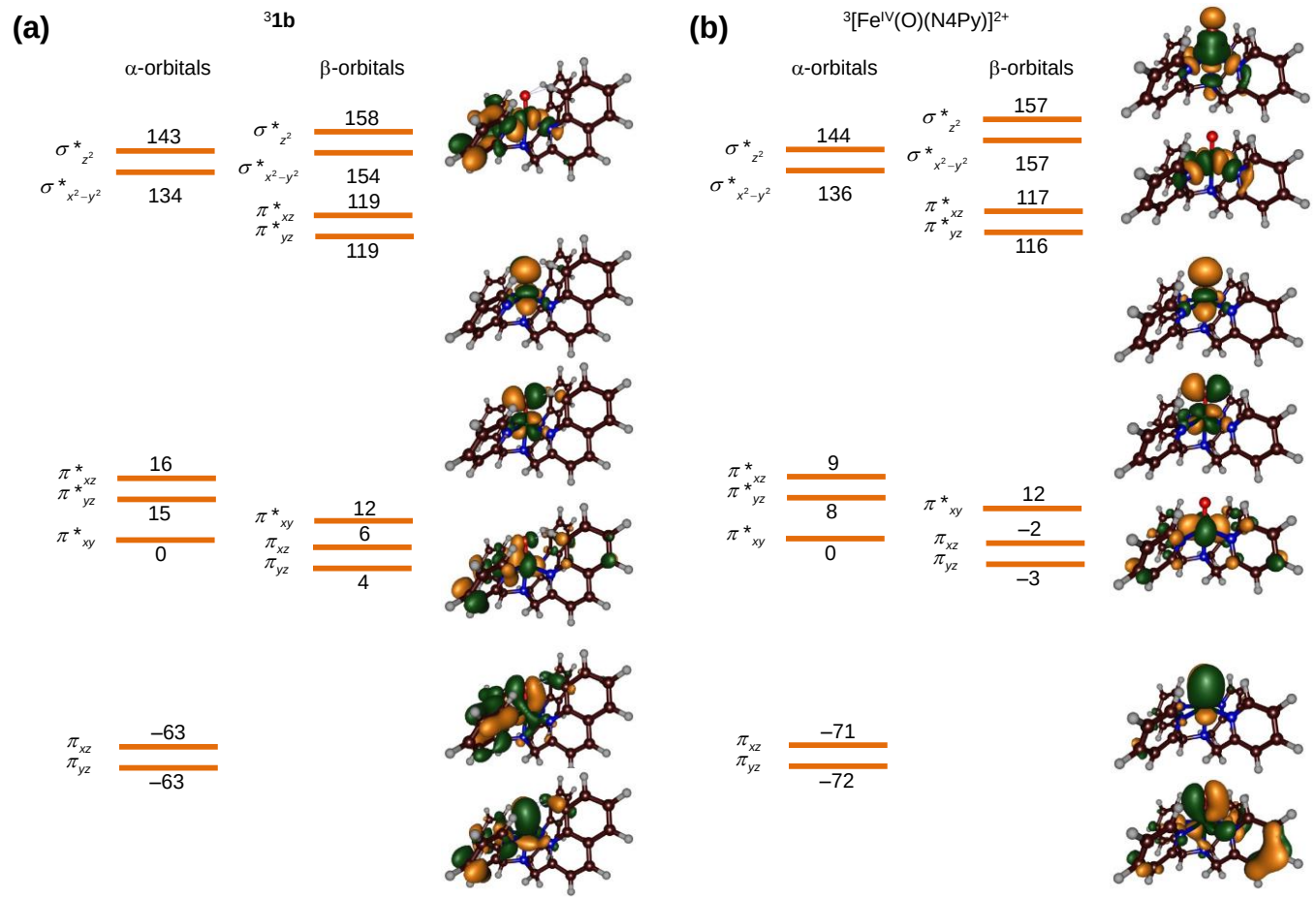

Fig. 6. Orbital energy levels of ^{3}**1b** (part a) and ^{3}**2b** (part b) as obtained at the UB3LYP/BS1 level of theory in Gaussian. Orbital energies are given in kcal mol^{-1} relative to the α-orbital for π^*_{xy}.

The molecular ground state in the triplet spin state is $\pi^*_{xy}{}^2$ $\pi^*_{xz}{}^1$ $\pi^*_{yz}{}^1$, whereas the quintet spin state has configuration $\pi^*_{xy}{}^1$ $\pi^*_{xz}{}^1$ $\pi^*_{yz}{}^1$ $\sigma^*_{x2-y2}{}^1$.

Orbital energies (Fig 6) are calculated relative to the π^*_{xy} orbital from the α-set of orbitals. As can be seen most relative energies are similar between the two structures and those for the π_{xz}/π_{yz} and π^*_{xz}/π^*_{yz} set of orbitals. These orbitals are all raised in energy in ^{3}**1b** as compared to ^{3}**2b**, which should lead to a lowering of the triplet-quintet energy gap as indeed found here. More dramatic changes are seen in the orbital shapes as depicted in Fig 6 alongside the orbital diagram. In particular, the π-orbitals of the pyridine ligands interact with the metal strongly in ^{3}**1b** and even the π^*_{xy} and σ^*_{x2-y2} orbitals are seen to be affected by this. Clearly, the equatorial ligand perturbation has a major effect on the molecular orbital shapes and energies that deviate dramatically from those typically found for pentadentate nonheme iron(IV)-oxo complexes without these effects.[33] Nevertheless, the molecular orbitals show clear metal-ligand interactions that affect the relative ordering and energies of the orbitals of the complex. As a result the triplet-quintet spin state gap is narrowed from 7.5 kcal mol^{-1} for $[Fe(O)(N4Py)]^{2+}$ to 2.8 kcal mol^{-1} for $[Fe(O)(2PyN2Q)]^{2+}$. This result is in line with Nordlander et al[18b] who also observed enhanced reactivities for hydrogen atom abstraction processes through equatorial ligand perturbations. In recent work, a nonheme iron(IV)-oxo complex with a tetra cyclic-NHC ligand was investigated, which showed considerable widening of the triplet and quintet spin states resulting in unexpected triplet spin reactivity patterns.[34] A reduced energy gap between triplet and quintet spin states is expected to enhance the reactivity dramatically.

Dalton Transactions

ARTICLE

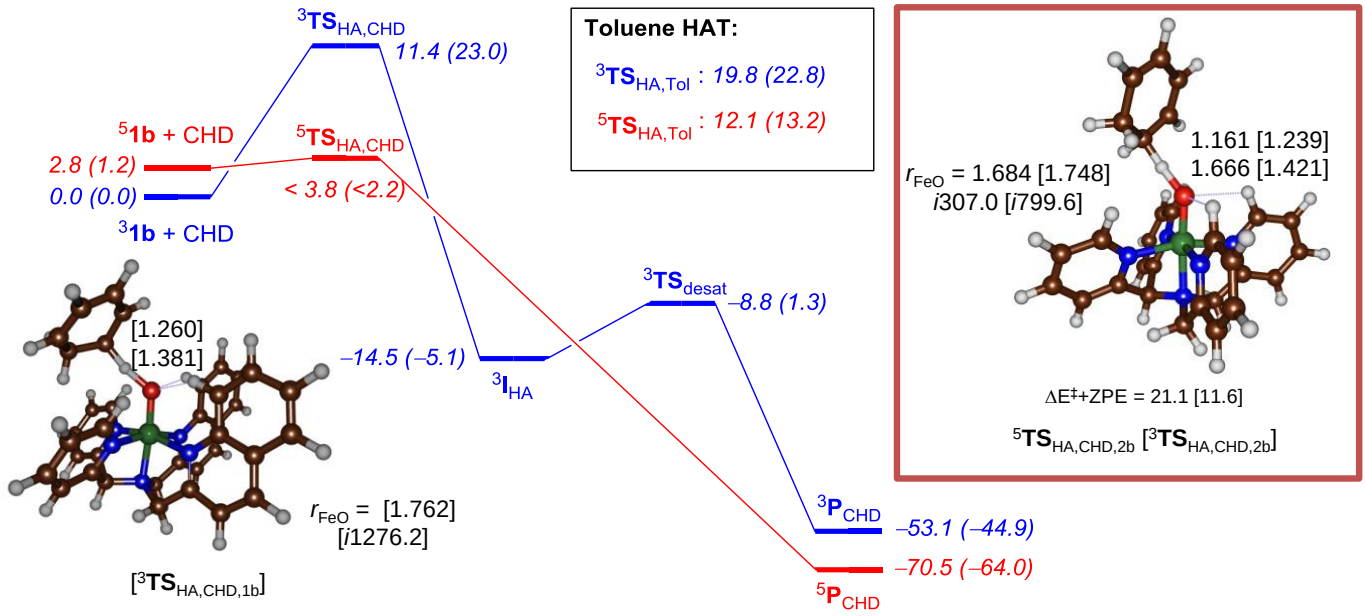

Fig. 7. Potential energy profile, $\Delta E+ZPE+E_{solv}$ and $\Delta G+E_{solv}$ (in parenthesis) with values in kcal mol^{-1} for CHD dehydrogenation and toluene hydrogen atom abstraction by ^{3,5}**1b** as calculated at UB3LYP/BS2//UB3LYP/BS1 level of theory. Also shown are optimized geometries of ^{3,5}**TS**$_{HA,CHD,1b}$ with bond lengths in angstroms, angles in degrees and the imaginary frequency in wave numbers. The value for ^{5}**TS**$_{HA,CHD}$ was estimated from the geometry scan.

Thus, in the triplet spin state a hydrogen atom abstraction results in filling of the π^*_{xz} orbital with a second electron, whereas in the quintet spin state the virtual σ^*_{z2} orbital is occupied. In most nonheme iron(III)-hydroxo complexes the intermediate with $\pi^*_{xy}{}^1\ \pi^*_{xz}{}^1\ \pi^*_{yz}{}^1\ \sigma^*_{x2-y2}{}^1\ \sigma^*_{z2}{}^1$ is the lowest in energy and hence the quintet pathway has the largest driving force.[35] As such, nonheme iron(IV)-oxo complexes react through two-state reactivity (TSR),[36] whereby in model complexes the reaction starts from a triplet spin state and cross over to the lower-lying quintet spin state during the reaction.

In our particular system, the ^{3,5}**1b** complex has a small triplet-quintet energy gap due to equatorial ligand perturbations that affect the structure and molecular orbitals along the Fe–O axis. Particularly, the change in O–Fe–N_{axial} angle will affect the $\sigma_{z2}/\sigma^*_{z2}$ orbital interactions of the oxo with iron atoms and particularly their energy levels and energy splitting. Since, the reduction of the iron(IV)-oxo complexes leads to filling of the σ^*_{z2} orbital with one electron this bending also should lower the energy of the complex to pick up an electron, i.e. its electron affinity (EA). As such, we calculated the electron affinities of **1b** as compared to **2b**. Indeed, we find a considerably lower electron affinity for **1b** than for **2b** as predicted: EA_{1b} = 123 kcal mol^{-1} and EA_{2b} = 134 kcal mol^{-1}. Therefore, the change in electron affinity should affect the reactivity differences with substrates as well in agreement with the experimental data reported above.

To further test the reactivity changes of **1b** versus **2b** with substrates for either hydrogen atom abstraction or oxygen atom transfer, we calculated the reaction mechanisms of **1b**/**2b** with several model substrates, namely 1,3-cyclohexadiene (CHD), toluene (Tol) and dimethylsulfide (DMS). These substrates were used in various previous studies with $[Fe^{IV}(O)(N4Py)]^{2+}$ and enable a direct comparison between the two oxidants, while toluene is one of the substrates reported above in our experimental study.

Let us first start with a discussion on the hydrogen atom abstraction from toluene and 1,3-cyclohexadiene by **1b** and **2b**. In particular, we investigated the dehydrogenation of 1,3-cyclohexadiene to benzene by ^{3,5}**1b** and ^{3,5}**2b**, and the results are given in Fig. 7. The reaction is stepwise with an initial hydrogen atom abstraction via transition state **TS**$_{HA}$ leading to a radical intermediate **Int**$_{HA}$. In the next step a second hydrogen atom abstraction occurs via transition state **TS**$_{reb}$ to form benzene products (**Prod**$_{HA}$). On the triplet spin state with oxidant **1b** as well as with both spin states for oxidant **2b** all these transition states and local minima could be characterized.

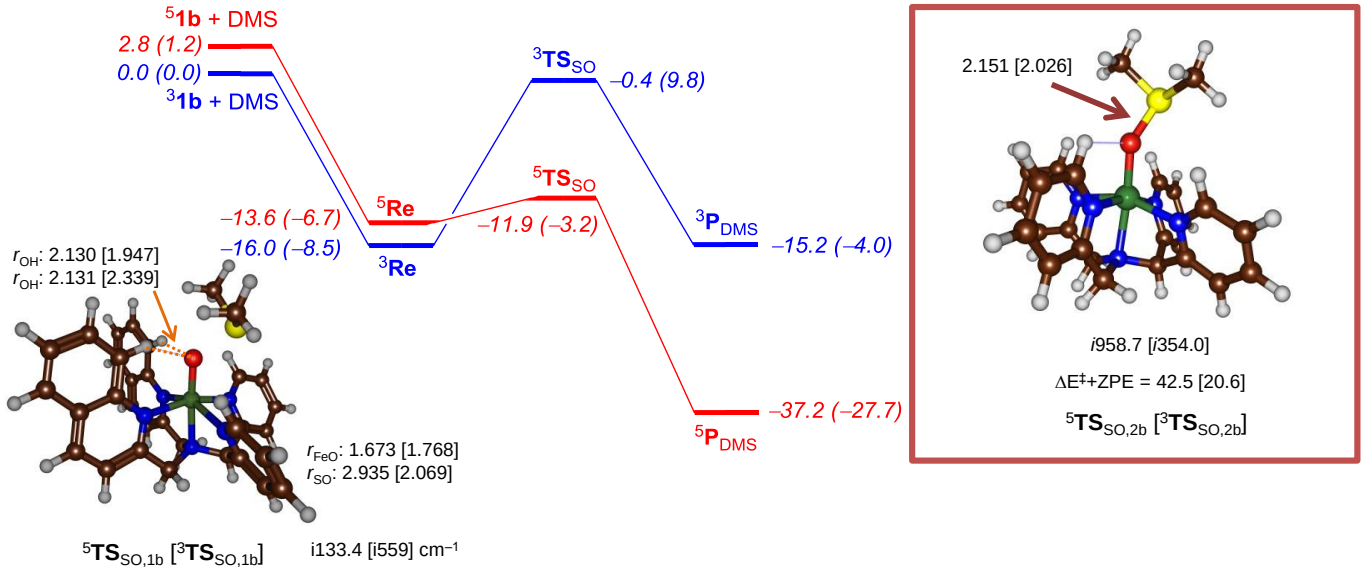

Fig. 8. Potential energy profile ($\Delta E+ZPE+E_{solv}$) with values in kcal mol^{-1} for DMS sulfoxidation by ^{3,5}**1b** as calculated at UB3LYP/BS2//UB3LYP/BS1 level of theory. Also shown are optimized geometries of ^{3,5}**TS**$_{SO,1b}$ with bond lengths in angstroms, angles in degrees and the imaginary frequency in wave numbers. The inset gives the ^{3,5}**TS**$_{SO,2b}$ optimized geometries from Ref 21.

However, starting from ^{5}**1b**, the reaction has an almost barrierless hydrogen atom abstraction transition state (that could not be characterized and was estimated from the geometry scan) and collapses to form products directly. This was established with detailed geometry scans that fixed one degree of freedom and optimized all others. As such the reaction will be facile on the quintet spin state and lead to products very rapidly.

As can be seen from Fig. 7, during the hydrogen atom abstraction a spin-state crossing occurs from the triplet to the quintet spin state to give the quintet spin products. With ^{3,5}**1b** this spin-state crossing is early and probably happens before the hydrogen atom abstraction transition state, so that ^{5}**TS**$_{HA,1b}$ will be rate-determining. On the triplet spin state the barrier is well higher in energy and located at 11.4 kcal mol^{-1} above ^{3}**Re**. These barriers are considerably lower than those found for ^{3}**2b** (^{5}**2b**) where values of 11.6 (21.1) kcal mol^{-1} were found. Previous calculations for this reaction found similar trends.[22] Therefore, the changes in molecular orbitals and the second-coordination sphere effects of the ligand present an ideal approach in the quintet spin state as well as significant triplet-quintet spin state separation. The combination of these effects raises the quintet barriers well above those for the triplet. Consequently, ^{3,5}**1b** will be a much better oxidant and is expected to react with substrates through hydrogen atom abstraction with significantly lower barriers than those reported for ^{3,5}**2b**. The experimental work reported above indeed confirms these calculations. Fig 7 gives barriers as calculated at $\Delta E+ZPE$ and ΔG level of theory. Similarly as seen before, thermal and entropy corrections to the enthalpy contribute to shift of about 10 kcal mol^{-1} and hence, on average ΔG values are 10 kcal mol^{-1} higher than $\Delta E+ZPE$ values.[37]

Optimized geometries of the hydrogen atom abstraction transition states are given in Fig. 7. The triplet spin structures are very similar with C–H and H–O distances of 1.239/1.421Å for ^{3}**TS**$_{HA,2b}$ versus 1.260/1.381Å for ^{3}**TS**$_{HA,1b}$. These structures match previously calculated hydrogen atom abstraction barrier well. Furthermore, the equatorial ligand perturbations of structure **1b** do not affect the geometry of the hydrogen atom abstraction barriers dramatically. Group spin densities of ^{3}**TS**$_{HA,1b}$ give a spin of 1.52 on the FeO unit and 0.51 on CHD, which implicates the transfer of a down-spin electron from substrate to π^*_{xz}. Indeed, the radical intermediate (^{3}**Int**$_{HA,1b}$) has configuration $\pi^*_{xy}{}^{2}\ \pi^*_{xz}{}^{2}\ \pi^*_{yz}{}^{1}\ \phi_{Sub}{}^{1}$. This type of mechanism has been labelled a $^{3}\pi$-pathway and usually proceeds via a transition state with a strongly bent angle of about 120° for the Fe–O–H interaction.[34,35] Our optimized geometry of ^{3}**TS**$_{HA,1b}$ is 127.2° in line with what is expected. Similar structure and electronic configuration was found for ^{3}**TS**$_{HA,2b}$.[22]

In the quintet spin state, by contrast, the hydrogen atom abstraction results in a transfer of an α-electron from substrate into the σ^*_{z2} orbital, which usually gives a radical intermediate with configuration $\pi^*_{xy}{}^{1}\ \pi^*_{xz}{}^{1}\ \pi^*_{yz}{}^{1}\ \sigma^*_{z2}{}^{1}\ \sigma^*_{x2-y2}{}^{1}\ \phi_{Sub}{}^{1}$, whereby all the unpaired electrons on the metal are up-spin and the substrate radical is down-spin. This mechanism is called the $^{5}\sigma$-pathway and generally gives a highly stable intermediate that is well below that of the triplet spin state. In the case of **1b** the radical intermediate is a shoulder on the potential energy profile and no stable, local minimum could be located. All attempts to optimize the structure of ^{5}**Int**$_{HA,1b}$ converged to the product complex instead.

Also given in Fig 7 are the hydrogen atom abstraction barriers from toluene by **1b**. In general, the barriers are considerably higher than those seen for 1,3-cyclohexadiene as a significantly stronger C–H bond is broken in the process. Indeed triplet and quintet spin free energies of activation of 22.8 and 13.2 kcal mol^{-1}, respectively for hydrogen atom abstraction from toluene are found. These values are in reasonable agreement with the rate constants reported in Table 2 above. Moreover, in comparison with the toluene hydrogen atom abstraction barriers by $[Fe^{IV}(O)(N4Py)]^{2+}$ reported previously,[31a] it implies a substantial rate-enhancement can be expected. This is in excellent agreement with the experimental rate-enhancement reported above.

To further understand the reactivity differences of **1b** and **2b** with substrates, we investigated oxygen atom transfer (OAT) to dimethylsulfide as a typical substrate for sulfoxidation reactions. Fig. 8 shows the potential energy landscape of OAT by ^{3,5}**1b** from DMS. As can be seen, the reaction proceeds by forming a reactant complex (^{3,5}**Re**) of oxidant and substrate in a highly exothermic reaction step of –16.0 kcal mol^{-1}, which retains the spin-state ordering between triplet and quintet. No charge transfer is encountered in this step and the electronic configuration stays the same as isolated reactants. Upon approach of the substrate on the oxo group an OAT transition state ($\mathbf{TS}_{SO}$) is encountered prior to the formation of the sulfoxide product complexes ($\mathbf{P}_{DMS}$). The quintet spin state barrier is very small (1.7 kcal mol^{-1} above ^{5}**Re**), whereas the triplet spin barrier is considerably higher in energy. Therefore, the reaction will proceed through a spin-state crossing from triplet to quintet during the OAT reaction. Moreover, these calculations imply much faster oxygen atom transfer than the bare N4Py complex, whereas the reactivity differences between **1b** and **2b** are much less for hydrogen atom abstraction in line with the experimental observations.

Previously,[22] we calculated a quintet spin barrier for OAT from $[Fe^{IV}(O)(N4Py)]^{2+}$ to DMS of 20.6 kcal mol^{-1} above a reactant complex. As such, the computational modelling agrees with a rate-enhancement upon replacing the oxidant of **2b** with **1b** as shown in Fig. 2b. Consequently, **1b** is a more efficient oxidant than **2b** because of a lower-lying quintet spin state that enables a fast spin-state crossing from triplet to quintet.

Optimized geometries of the oxygen atom transfer transition states using ^{3,5}**1b** and ^{3,5}**2b** as oxidants are shown in Fig. 8. These transition states show typical features of sulfoxidation transition states seen before with elongated Fe–O and O–S bonds.[38] In the $^{3}\mathbf{TS}_{SO,1b}$ the Fe–O and O–S distances are 1.768 and 2.069 Å and hence the transition state is late on the potential energy surface. By contrast, the quintet spin state transition state is much earlier with a very long O–S distance of 2.935 Å and still a relatively short Fe–O distance of 1.673 Å. The quintet spin state structure has a small imaginary frequency of i133 cm^{-1}, while a much larger value was obtained with model **2b**. Therefore, considerable differences of the potential energy profile are seen through the modification of the N4Py ligand system with aromatic rings that clearly affect substrate approach and activation.

In summary, the DFT calculations show that ^{3,5}**1b** is much more reactive with substrates than ^{3,5}**2b**. This is the result from changes in the σ_{z2} and σ^*_{z2} molecular orbitals, which are perturbed by equatorial interactions particularly of C–H groups to the oxo. As a consequence, the electron affinity of **1b** is significantly lower than that of **2b** and hence it is more reactive.

Experimental

Materials and methods.

All Chemicals were obtained from Aldrich Chemical Co., and were of the best available purity and used without further purification unless otherwise stated. Solvents were dried according to published procedures[39] and distilled under argon prior to use. $H_2{}^{18}O$ (99.9% pure and enrichment 97.1 atom%) was purchased from Berry and Associates (Icon Isotopes). Benzyl alcohol-d_7 was purchased from Cambridge Isotope Laboratories, Inc. Iodosylbenzene and 1-^{t}butylsulfonyl-2-iodosylbenzene were prepared using previously reported literature methods.[40] The ligand (2PyN2Q) was synthesized using previously reported procedures.[18a] Iron(II) complex, $[Fe^{II}(2PyN2Q)](CF_3SO_3)_2$, (**1a**) was synthesized inside a glove-box by an equimolar reaction of 2PyN2Q and $Fe^{II}(CF_3SO_3)_2{\bullet}2CH_3CN$ in CH_3CN. The reaction mixture was stirred overnight, filtered with the help of syringe filters. Excess diethyl ether was slowly added to the resulting filtrate and the bilayer solution was left undisturbed inside the glovebox at –40 °C. The ethereal solution was decanted off after a few days and the yellowish residue was washed several times with diethyl ether and dried under vacuum to get the desired complex **1a** in excellent yield (95%). The $[Fe^{IV}(O)(2PyN2Q)]^{2+}$ (**1b**) was synthesized in situ in CH_3CN by adding 1.5 equivalents of $PhI(OAc)_2$ in CH_3CN at ambient temperature and was further used for all the kinetic studies. The $[Fe^{II}(N4Py)](CF_3SO_3)_2$ complex (**2a**) and corresponding $[Fe^{IV}(O)(N4Py)]^{2+}$ intermediate (**2b**) were synthesized by previously reported procedures.[12,13]

Instrumentation.

Bruker Avance III HD 600 and 400 MHz NMR spectrometers were used for recording NMR spectra using TMS as an internal standard. Variable temperature-NMR spectra were recorded on a Jeol Advanced Solution State 400 MHz spectrometer (JNM ECZ400S). UV-vis spectra were recorded on a Hewlett Packard 8453 spectrophotometer equipped with either constant temperature circulating water bath or a liquid nitrogen cryostat (Unisoku) with a temperature controller. The purified complexes and intermediates were characterized by mass spectrometry on Agilent-Q-TOF 6520 instrument in positive ESI mode equipped with a Mass hunter workstation. The samples were infused directly into the source. The spray voltage was set at 3 kV and the drying gas flow and temperature were maintained as 5.0 L min^{-1} and 200 °C respectively. The products were analysed by ^{1}H and ^{13}C-NMR recorded with Bruker Avance III HD 600 and 400 MHz spectrometers and

LCMS with Waters ACQUITY UPLC equipped with a variable wavelength UV-200 detector. Product yields were determined by comparison with standard curves of authentic samples.

Reactivity studies.

All reactions were run in a 10 mm path length UV-vis cuvette by monitoring UV-vis spectral changes of reaction solutions. The kinetics studies were performed under pseudo first-order conditions with excess substrate in acetonitrile. The reactions were monitored by following the decrease of the absorbance of the characteristic peaks as a function of time. The rate constants were determined by fitting the changes in absorbance of the intermediates under study. Reactions were run at least in triplicate and the data reported represents the average of those.

Computational modelling.

Computational studies used density functional theory as implemented in the Gaussian program package.[41] Due to the overall charge of +2 in our chemical system full geometry optimizations were performed with a solvent model, i.e. the polarized continuum model mimicking acetonitrile. We did initial optimizations and frequency calculations using the hybrid density functional method UB3LYP and the LACVP basis set on iron and 6-31G on the rest of the atoms (BS1).[42,43] Subsequent single points utilized a triple-ζ LACV3P+ basis set on iron and 6-311+G* on the rest of the atoms (BS2). All structures were calculated on the lowest lying triplet and quintet spin state surfaces and all structures were characterized by a frequency calculation at the same level of theory as the optimization as either a local minimum (without imaginary frequencies) or a transition state structure (with one imaginary frequency for the correct mode). Reactivities were investigated with dimethylsulfide (DMS), cyclohexadiene (CHD) and toluene (Tol) as model substrates for sulfoxidation and HAT reactions.

Conclusions

In conclusion, we have synthesized a room temperature stable iron(IV)-oxo intermediate (**1b**) that acts as an efficient oxidant of substrates. Instead of contributing to the steric fencing around the iron(IV)-oxo core and prohibiting molecular approach, the introduction of two bulky quinoline groups in the N4Py ligand framework has notably enhanced the HAT and OAT reactivity of the iron(IV)-oxo complex. We did a comparative study of thioanisole oxidation and hydrogen atom abstraction reactions with various substrates. We show that **1b** reacts with substrates with increased rate constants with respect to those obtained with oxidant **2b** which is attributed to subtle changes in the ligand skeleton that position the oxo group and lower the virtual σ^*_{z2} orbital in energy. These engineered structures show that small perturbations on the equatorial ligand may have major influences in substrate positioning and reactivity in line with what is found for enzymatic reaction mechanisms. The work highlights how tweaking the ligand architecture of a catalyst can affect its performance, which will help in designing novel synthetic scaffolds for enzymatic mimics.

Conflicts of interest

There are no conflicts to declare.

Acknowledgements

CVS acknowledges financial support by Department of Science and Technology (SERB), India (EMR/2014/000279). CSIR-IICB is duly acknowledged for providing access to VT-NMR equipment. SdV and CVS thank the British Council for a UK-India Education Research Initiative (UKIERI) award (DST/INT/UK/P-151/2017). FC thanks the Conacyt Mexico for a studentship. DK acknowledges financial support from the DBT, New Delhi (BT/PR14510/BID/07/334/2010).

Notes and references

1 a) E. I. Solomon, T. C. Brunold, M. I. Davis, J. N. Kemsley, S. K. Lee, N. Lehnert, F. Neese, A. J. Skulan, Y. S. Yang and J. Zhou, *Chem. Rev*., 2000, **100**, 235; b) M. Costas, M. P. Mehn, M. P. Jensen and L. Que Jr., *Chem. Rev*., 2004, **104**, 939; c) M. M. Abu-Omar, A. Loaiza and N. Hontzeas, *Chem. Rev*., 2005, **105**, 2227; d) P. C. A. Bruijnincx, G. van Koten and R. J. M. Klein Gebbink, *Chem. Soc. Rev*., 2008, **37**, 2716; e) A. R. McDonald and L. Que Jr, *Coord. Chem. Rev*., 2013, **257**, 414; f) W. Nam, Y.-M. Lee and S. Fukuzumi, *Acc. Chem. Res*., 2014, **47**, 1146.

2 a) M. Sono, M. P. Roach, E. D. Coulter and J. H. Dawson, *Chem. Rev.*, 1996, **96**, 2841; b) J. T. Groves, *Proc. Natl. Acad. Sci. USA*, 2003, **100**, 3569; c) B. Meunier, S. P. de Visser and S. Shaik, *Chem. Rev*., 2004, **104**, 3947; d) I. G. Denisov, T. M. Makris, S. G. Sligar and I. Schlichting, *Chem. Rev*., 2005, **105**, 2253; e) S. V. Kryatov, E. V. Rybak-Akimova and S. Schindler, *Chem. Rev*., 2005, **105**, 2175; f) R. van Eldik, *Coord. Chem. Rev*., 2007, **251**, 1649; g) P. R. Ortiz de Montellano, *Chem. Rev*., 2010, **110**, 932; h) *Iron-containing enzymes: Versatile catalysts of hydroxylation reactions in nature* (Eds.: S. P. de Visser and D. Kumar), RSC Publishing, Cambridge, 2011.

3 a) D. A. Proshlyakov, T. F. Henshaw, G. R. Monterosso, M. J. Ryle and R. P. Hausinger, *J. Am. Chem. Soc*., 2004, **126**, 1022; b) J. M. Bollinger Jr, J. C. Price, L. M. Hoffart, E. W. Barr and C. Krebs, *Eur. J. Inorg. Chem*., 2005, 4245.

4 a) K. Gorres and R. T. Raines, *Crit. Rev. Biochem. Mol. Biol.*, 2010, **45**, 106; b) M. A. McDonough, V. Li, E. Flashman, R. Chowdhury, C. Mohr, B. M. Lienard, J. Zondlo, N. J. Oldham, I. J. Clifton, J. Lewis, L. A. McNeill, R. J. Kurzeja, K. S. Hewitson, E. Yang, S. Jordan, R. S. Syed and C. J. Schofield, *Proc. Natl. Acad. Sci. USA*, 2006, **103**, 9814.

5 a) A. Timmins, M. Saint-André and S. P. de Visser, *J. Am. Chem. Soc*., 2017, **139**, 9855; b) A. Timmins and S. P. de Visser, *Frontiers Chem*. **2017**, *5*, Article 94, pp 1–13, doi: 10.3389/fchem.2017.00094.

6 See, e.g., R. Davydov, T. M. Makris, V. Kofman, D. E. Werst, S. G. Sligar and B. M. Hoffman, *J. Am. Chem. Soc*., 2001, **123**, 1403.

7 a) P. J. O'Brien, *Chem. Rev*., 2006, **106**, 720; b) C. Yi, C. G. Yang and C. He, *Acc. Chem. Res*., 2009, **42**, 519.

8 a) M. Atanasov, P. Comba, S. Hausberg and B. Martin, *Coord. Chem. Rev*., 2009, **253**, 2306; b) M. Costas, *Coord. Chem. Rev*., 2011, **255**, 2912; c) C. V. Sastri, J. Lee, K. Oh, Y. J. Lee, J.

Lee, T. A. Jackson, K. Ray, H. Hirao, W. Shin, J. A. Halfen, J. Kim, L. Que Jr., S. Shaik and W. Nam, *Proc. Natl. Acad. Sci. USA*, 2007, **104**, 19181; d) C. Buron, K. Sénéchal-David, R. Ricoux, J.-P. Le Caër, V. Guérineau, P. Méjanelle, R. Guillot, C. Herrero, J.-P. Mahy and F. Banse, *Chem. Eur. J.*, 2015, **21**, 12188; e) X. Engelmann, I. Monte-Pérez and K. Ray, *Angew. Chem. Int. Ed*., 2016, **55**, 7632.

9 See, e.g., a) I. Prat, L. Gómez, M. Canta, X. Ribas and M. Costas, *Chem. Eur. J*., 2013, **19**, 1908; b) M. G. Quesne, D. Senthilnathan, D. Singh, D. Kumar, P. Maldivi, A. B. Sorokin and S. P. de Visser, *ACS Catal*., 2016, **6**, 2230; c) P. Barman, A. S. Faponle, A. K. Vardhaman, D. Angelone, A.-M. Löhr, W. R. Browne, P. Comba, C. V. Sastri and S. P. de Visser, *Inorg. Chem*., 2016, **55**, 10170; d) S. P. de Visser, L. Tahsini and W. Nam, *Chem. Eur. J*., 2009, **15**, 5577; e) J. Annaraj, J. Cho, Y.-M. Lee, S. Y. Kim, R. Latifi, S. P. de Visser and W. Nam, *Angew. Chem. Int. Ed*., 2009, **48**, 4150; f) A. Takahashi, D. Yamaki, K. Ikemura, T. Kurahashi, T. Ogura, M. Hada and H. Fujii, *Inorg. Chem*., 2012, **51**, 7296; g) T. A. Jackson, J.-U. Rohde, M. S. Seo, C. V. Sastri, R. DeHont, A. Stubna, T. Ohta, T. Kitagawa, E. Münck, W. Nam and L. Que Jr, *J. Am. Chem. Soc*., 2008, **130**, 12394.

10 a) S. Sahu, L. R. Widger, M. G. Quesne, S. P. de Visser, H. Matsumura, P. Moënne-Loccoz, M. A. Siegler and D. P. Goldberg, *J. Am. Chem. Soc*., 2013, **135**, 10590; b) D. C. Lacy, R. Gupta, K. L. Stone, J. Greaves, J. W. Ziller, M. P. Hendrich and A. S. Borovik, *J. Am. Chem. Soc*., 2010, **132**, 12188; c) Ü. İşci, A. S. Faponle, P. Afanasiev, F. Albrieux, V. Briois, V. Ahsen, F. Dumoulin, A. B. Sorokin and S. P. de Visser, *Chem. Sci*., 2015, **6**, 5063; d) J.-G. Liu, T. Ohta, S. Yamaguchi, T. Ogura, S. Sakamoto, Y. Maeda and Y. Naruta, *Angew. Chem. Int. Ed*., 2009, **48**, 9262; e) T. Taguchi, R. Gupta, B. Lassalle-Kaiser, D. W. Boyce, V. K. Yachandra, W. B. Tolman, J. Yano, M. P. Hendrich and A. S. Borovik, *J. Am. Chem. Soc*., 2012, **134**, 1996; f) Z. Gordon, M. J. Drummond, E. M. Matson, J. A. Bogart, E. J. Schelter, R. L. Lord and A. R. Fout, *Inorg. Chem*., 2017, **56**, 4852; g) M. Sørensen Vad, A. Lennartson, A. Nielsen, J. Harmer, J. E. McGrady, C. Frandsen, S. Mørup and C. J. McKenzie, *Chem. Commun*., 2012, **48**, 10880; h) F. Wang, W. Sun, C. Xia and Y. Wang, *J. Biol. Inorg. Chem*., 2017, **22**, 987; i) F. Burg, M. Gicquel, S. Breitenlechner, A. Pöthig and T. Bach, *Angew. Chem. Int. Ed*., 2018, **57**, 2953.

11 See, e.g., a) C. E. MacBeth, R. Gupta, K. R. Mitchell-Koch, V. G. Young Jr., G. H. Lushington, W. H. Thompson, M. P. Hendrich and A. S. Borovik, *J. Am. Chem. Soc*., 2004, **126**, 2556; b) T. Ishizuka, S. Ohzu, H. Kotani, Y. Shiota, K. Yoshizawa and T. Kojima, *Chem. Sci*., 2014, **5**, 1429; c) M. Mitra, J. Lloret-Fillol, M. Haukka, M. Costas and E. Nordlander, *Chem. Commun*., 2014, **50**, 1408.

12 M. Lubben, A. Meetsma, E. C. Wilkinson, B. Feringa and L. Que Jr., *Angew. Chem. Int. Ed.*, 1995, **34**, 1512.

13 a) J. Kaizer, E. J. Klinker, N. Y. Oh, J.-U. Rohde, W. J. Song, A. Stubna, J. Kim, E. Münck, W. Nam and L. Que Jr, *J. Am. Chem. Soc*., 2004, **126**, 472; b) E. J. Klinker, J. Kaizer, W. W. Brennessel, N. L. Woodrum, C. J. Cramer and L. Que Jr, *Angew. Chem. Int. Ed*., 2005, **44**, 3690.

14 See, e.g., a) D. Lakk-Bogáth, R. Csonka, G. Speier, M. Réglier, A. J. Simaan, J.-V. Naubron, M. Giorgi, K. Lázár and J. Kaizer, *Inorg. Chem*., 2016, **55**, 10090; b) S. K. Padamati, A. Draksharapu, D. Unjaroen and W. R. Browne, *Inorg. Chem*., 2016, **55**, 4211; c) S. Kim, K.-B. Cho, Y.-M. Lee, J. Chen, S. Fukuzumi and W. Nam, *J. Am. Chem. Soc*., 2016, **138**, 10654; d) D. Wang, K. Ray, M. J. Collins, E. R. Farquhar, J. R. Frisch, L. Gómez, T. A. Jackson, M. Kerscher, A. Waleska, P. Comba, M. Costas and L. Que Jr, *Chem. Sci*., 2013, **4**, 282; e) A. Draksharapu, D. Angelone, M. G. Quesne, S. K. Padamati, L. Gómez, R. Hage, M. Costas, W. R. Browne and S. P. de Visser, *Angew. Chem. Int. Ed*., 2015, **54**, 4357; f) A. K. Vardhaman, P. Barman, S. Kumar, C. V. Sastri, D. Kumar and S. P. de Visser, *Chem. Commun*., 2013, **49**, 10926; g) C. V. Sastri, K. Oh, Y. J. Lee, M. S. Seo, W. Shin and W. Nam, *Angew. Chem. Int. Ed*., 2006, **45**, 3992; h) S. P. de Visser, Y.-M. Lee and W. Nam, *Eur. J. Inorg. Chem*., 2008, 1027; i) J. Park, Y. Morimoto, Y.-M. Lee, W. Nam and S. Fukuzumi, *J. Am. Chem. Soc*., 2011, **133**, 5236; j) K. Benzing, P. Comba, B. Martin, B. Pokrandt and F. Keppler, *Chem. Eur. J.,* 2017, **23**, 10465; k) R. Turcas, D. Lakk-Bogáth, G. Speier and J. Kaizer, *Dalton. Trans*., 2018, **47**, 3248.

15 A. N. Biswas, M. Puri, K. K. Meier, W. N. Oloo, G. T. Rohde, E. L. Bominaar, E. Münck and L. Que Jr, *J. Am. Chem. Soc.,* 2015, **137**, 2428.

16 M. S. Seo, N. H. Kim, K. B. Cho, J. E. So, S. K. Park, M. Clémancey, R. G. Serres, J. M. Latour, S. Shaik and W. Nam, *Chem. Sci*., 2011, **2**, 1039.

17 M. Mitra, H. Nimir, S. Demeshko, S. S. Bhat, S. O. Malinkin, M. Haukka, J. Lloret-Fillol, G. C. Lisensky, F. Meyer, A. A. Shteinman, W. R. Browne, D. A. Hrovat, M. G. Richmond, M. Costas and E. Nordlander, *Inorg. Chem*., 2015, **54**, 7152.

18 a) W. K. C. Lo, C. J. McAdam, A. G. Blackman, J. D. Crowley and D. A. McMorran, *Inorg. Chim. Acta*, 2015, **426**, 183; b) A. A. Massie, M. C. Denler, L. T. Cardoso, A. N. Walker, M. K. Hossain, V. W. Day, E. Nordlander and T. A. Jackson, *Angew. Chem. Int. Ed*., 2017, **56**, 4178; c) A. A. Massie, A. Sinha, J. D. Parham, E. Nordlander and T. A. Jackson, *Inorg. Chem.*, 2018, **57**, 8253.

19 W. Rasheed, A. Draksharapu, S. Banerjee, V. G. Young Jr, R. Fan, Y. Guo, M. Ozerov, J. Nehrkorn, J. Krzystek, J. Telser and L. Que Jr, *Angew. Chem. Int. Ed*., 2018, **57**, 9387.

20 a) K. Ray, J. England, A. T. Fiedler, M. Martinho, E. Münck and L. Que Jr, *Angew. Chem. Int. Ed.*, 2008, **47**, 8068; b) A. Company, G. Sabenya, M. González-Béjar, L. Gómez, M. Clémancey, G. Blondin, A. J. Jasniewski, M. Puri, W. S. Browne, J. M. Latour, L. Que Jr., M. Costas, J. Pérez-Prieto and J. Lloret-Fillol, *J. Am. Chem. Soc.*, 2014, **136**, 4624; c) S. Sahu, M. G. Quesne, C. G. Davies, M. Dürr, I. Ivanović-Burmazović, M. A. Siegler, G. N. L. Jameson, S. P. de Visser and D. P. Goldberg, *J. Am. Chem. Soc.*, 2014, **136**, 13542; d) L. R. Widger, C. G. Davies, T. Yang, M. A. Siegler, O. Troeppner, G. N. L. Jameson, I. Ivanović-Burmazović and D. P. Goldberg, *J. Am. Chem. Soc.*, 2014, **136**, 2699; e) S. Sahu, B. Zhang, C. J. Pollock, M. Dürr, C. G. Davies, A. M. Confer, I. Ivanović-Burmazović, M. A. Siegler, G. N. L. Jameson, C. Krebs and D. P. Goldberg, *J. Am. Chem. Soc.*, 2016, **138**, 12791.

21 a) H. C. Brown and Y. Okamoto, *J. Am. Chem. Soc*., 1958, **80**, 4979; b) Y. Goto, T. Matsui, S. I. Ozaki, Y. Watanabe and S. Fukuzumi, *J. Am. Chem. Soc*., 1999, **121**, 9497.

22 S. Kumar, A. S. Faponle, P. Barman, A. K. Vardhaman, C. V. Sastri, D. Kumar and S. P. de Visser, *J. Am. Chem. Soc*., 2014, **136**, 17102.

23 N. Y. Oh, Y. Suh, M. J. Park, M. S. Seo, J. Kim and W. Nam, *Angew. Chem. Int. Ed*., 2005, **44**, 4235.

24 a) L. E. Friedrich, *J. Org. Chem*., 1983, **48**, 3851; b) F. G. Bordwell and J.-P. Cheng, *J. Am. Chem. Soc*., 1991, **113**, 1736; c) J. M. Mayer, *Acc. Chem. Res*., 1998, **31**, 441; d) J. M. Mayer, *Annu. Rev. Phys. Chem*., 2004, **55**, 363.

25 a) J. Yoon, S. A. Wilson, Y. K. Jang, M. S. Seo, K. Nehru, B. Hedman, K. O. Hodgson, E. Bill, E. I. Solomon and W. Nam, *Angew. Chem. Int. Ed*., 2009, **48**, 1257; b) D. E. Lansky and D. P. Goldberg, *Inorg. Chem*., 2006, **45**, 5119; c) A. J. McGown, W. D. Kerber, H. Fujii and D. P. Goldberg, *J. Am. Chem. Soc*., 2009, **131**, 8040; d) S. R. Bell and J. T. Groves, *J. Am. Chem. Soc*., 2009, **131**, 9640; e) Y. Kang, H. Chen, Y. J. Jeong, W. Lai, E. H. Bae, S. Shaik and W. Nam, *Chem. Eur. J*., 2009, **15**, 10039; f) J. J. Warren, T. A. Tronic and J. M. Mayer, *Chem. Rev*., 2010, **110**, 6961; g) K. A. Prokop, S. P. de Visser and D. P. Goldberg, *Angew. Chem. Int. Ed*., 2010, **49**, 5091; h) J. M.

Mayer, E. A. Mader, J. P. Roth, J. R. Bryant, T. Matsuo, A. Dehestani, B. C. Bales, E. J. Watson, T. Osako, K. Valliant-Saunders, W. H. Lam, D. A. Hrovat, W. T. Borden and E. R. Davidson, *J. Mol. Catal. A*, 2006, **251**, 24; i) C. Arunkumar, Y. M. Lee, J. Y. Lee, S. Fukuzumi and W. Nam, *Chem. Eur. J.*, 2009, **15**, 11482; j) A. K. Vardhaman, P. Barman, S. Kumar, C. V. Sastri, D. Kumar and S. P. de Visser, *Angew. Chem. Int. Ed*., 2013, **52**, 12288.

26 See, e.g., T. Yang, M. G. Quesne, H. M. Neu, F. G. Cantú Reinhard, D. P. Goldberg and S. P. de Visser, *J. Am. Chem. Soc*., 2016, **138**, 12375.

27 a) A. K. Vardhaman, C. V. Sastri, D. Kumar and S. P. de Visser, *Chem. Commun*., 2011, **47**, 11044; b) F. G. Cantú Reinhard, A. S. Faponle and S. P. de Visser, *J. Phys. Chem. A*, 2016, **120**, 9805.

28 a) M. A. Sainna, S. Kumar, D. Kumar, S. Fornarini, M. E. Crestoni and S. P. de Visser, *Chem. Sci*., 2015, **6**, 1516; b) F. G. Cantú Reinhard, M. A. Sainna, P. Upadhyay, G. A. Balan, D. Kumar, S. Fornarini, M. E. Crestoni and S. P. de Visser, *Chem. Eur. J*., 2016, **22**, 18608.

29 a) S. P. de Visser, *J. Am. Chem. Soc*., 2010, **132**, 1087; b) M. A. Kaczmarek, A. Malhotra, G. A. Balan, A. Timmins and S. P. de Visser, *Chem. Eur. J*., 2018, **24**, 5293; c) A. Timmins, M. G. Quesne, T. Borowski and S. P. de Visser, *ACS Catal*., **2018**, 8 accepted; DOI: 10.1021/acscatal.8b01673.

30 a) L. Ji, A. S. Faponle, M. G. Quesne, M. A. Sainna, J. Zhang, A. Franke, D. Kumar, R. van Eldik, W. Liu and S. P. de Visser, *Chem. Eur. J*., 2015, **21**, 9083; b) B. Karamzadeh, D. Kumar, G. N. Sastry and S. P. de Visser, *J. Phys. Chem. A*, 2010, **114**, 13234.

31 a) D. Kumar, H. Hirao, L. Que Jr and S. Shaik, *J. Am. Chem. Soc*., 2005, **127**, 8026; b) T. Z. H. Gani and H. J. Kulik, *ACS Catal*., 2018, **8**, 975.

32 a) S. P. de Visser, S. Shaik, P. K. Sharma, D. Kumar and W. Thiel, *J. Am. Chem. Soc*., 2003, **125**, 15779; b) X.-X. Li, V. Postils, W. Sun, A. S. Faponle, M. Solà, Y. Wang, W. Nam and S. P. de Visser, *Chem. Eur. J*., 2017, **23**, 6406.

33 a) L. Bernasconi and E.-J. Baerends, *J. Am. Chem. Soc*., 2013, **135**, 8857; b) Y. Liu, X. Guan, E. L.-M. Wong, P. Liu, J.-S. Huang and C.-M. Che, *J. Am. Chem. Soc*., 2013, **135**, 7194; c) A. Dey, *J. Am. Chem. Soc*., 2010, **132**, 13892; d) H. Hirao, F. Li, L. Que Jr and K. Morokuma, *Inorg. Chem*., 2011, **50**, 6637; e) D. Usharani, D. C. Lacy, A. S. Borovik and S. Shaik, *J. Am. Chem. Soc*., 2013, **135**, 17090; f) S. P. de Visser, *J. Am. Chem. Soc*., 2006, **128**, 9813.

34 a) F. G. Cantú Reinhard and S. P. de Visser, *Chem. Eur. J.*, 2017, **23**, 2935; b) R. Latifi, M. A. Sainna, E. V. Rybak-Akimova and S. P. de Visser, *Chem. Eur. J*., 2013, **19**, 4058; c) M. G. Quesne, R. Latifi, L. E. Gonzalez-Ovalle, D. Kumar and S. P. de Visser, *Chem. Eur. J*., 2014, **20**, 435.

35 a) L. Bernasconi and E. J. Baerends, *Eur. J. Inorg. Chem*., 2008, 1672; b) S. P. de Visser, *J. Am. Chem. Soc*., 2006, **128**, 15809; c) S. Ye and F. Neese, *Proc. Natl. Acad. Sci. USA*, 2011, **108**, 1228; d) H. Tang, J. Guan, H. Liu and X. Huang, *Dalton Trans*., 2013, **42**, 10260; e) A. Ansari, A. Kaushik and G. Rajaraman, *J. Am. Chem. Soc*., 2013, **135**, 4235.

36 a) S. Shaik, H. Chen and D. Janardanan, *Nat. Chem*., 2011, **3**, 19; b) C. T. Saouma and J. M. Mayer, *Chem. Sci*., 2014, **5**, 21.

37 a) D. Kumar, B. Karamzadeh, G. N. Sastry and S. P. de Visser, *J. Am. Chem. Soc*., **2010**, *132*, 7656; b) D. Kumar, R. Latifi, S. Kumar, E. V. Rybak-Akimova, M. A. Sainna and S. P. de Visser, *Inorg. Chem*., **2013**, *52*, 7968.

38 a) D. Kumar, G. N. Sastry and S. P. de Visser, *Chem. Eur. J.*, 2011, **17**, 6196; b) A. S. Faponle, F. P. Seebeck and S. P. de Visser, *J. Am. Chem. Soc*., 2017, **139**, 9259.

39 *Purification of Laboratory Chemicals*, W. L. F. Armarego and D. D. Perrin (Eds.); Pergamon Press, Oxford, 1997.

40 a) *Organic Syntheses*, H. Saltzman and J. G. Sharefkin (Eds.); Wiley, New York, 1973, Collect. Vol. V, pp. 658; b) D. Macikenas, E. Skrzypczak-Jankun and J. D. Protasiewicz, *J. Am. Chem. Soc.*, 1999, **121**, 7164.

41 Gaussian 09, Revision C.01, M. J. Frisch, G. W. Trucks, H. B. Schlegel, G. E. Scuseria, M. A. Robb, J. R. Cheeseman, G. Scalmani, V. Barone, B. Mennucci, G. A. Petersson, H. Nakatsuji, M. Caricato, X. Li, H. P. Hratchian, A. F. Izmaylov, J. Bloino, G. Zheng, J. L. Sonnenberg, M. Hada, M. Ehara, K. Toyota, R. Fukuda, J. Hasegawa, M. Ishida, T. Nakajima, Y. Honda, O. Kitao, H. Nakai, T. Vreven, J. A. Montgomery, Jr., J. E. Peralta, F. Ogliaro, M. Bearpark, J. J. Heyd, E. Brothers, K. N. Kudin, V. N. Staroverov, T. Keith, R. Kobayashi, J. Normand, K. Raghavachari, A. Rendell, J. C. Burant, S. S. Iyengar, J. Tomasi, M. Cossi, N. Rega, J. M. Millam, M. Klene, J. E. Knox, J. B. Cross, V. Bakken, C. Adamo, J. Jaramillo, R. Gomperts, R. E. Stratmann, O. Yazyev, A. J. Austin, R. Cammi, C. Pomelli, J. W. Ochterski, R. L. Martin, K. Morokuma, V. G. Zakrzewski, G. A. Voth, P. Salvador, J. J. Dannenberg, S. Dapprich, A. D. Daniels, O. Farkas, J. B. Foresman, J. V. Ortiz, J. Cioslowski and D. J. Fox, Gaussian, Inc., Wallingford CT, 2010.

42 a) A. D. Becke, *J. Chem. Phys*., 1993, **98**, 5648; b) C. Lee, W. Yang and R. G. Parr, *Phys. Rev. B*, 1988, **37**, 785.

43 a) P. J. Hay and W. R. Wadt, *J. Chem. Phys*., 1985, **82**, 270; b) W. J. Hehre, R. Ditchfield and J. A. Pople, *J. Chem. Phys*., 1972, **56**, 2257.

Table of Contents Artwork: